Dynamics of Oxide Growth on Pt Nanoparticles Electrodes in the Presence of Competing Halides by Operando Energy Dispersive X-Ray Absorption Spectroscopy

Alessandro Minguzzi[a,b] *, Linda Montagna[c,†], Andrea Falqui[d], Alberto Vertova[a,b], Sandra Rondinini[a,b], Paolo Ghigna[b,c]

[a] Dipartimento di Chimica, Università degli Studi di Milano, via Golgi 19, 20133, Milano, Italy

[b] Consorzio Interuniversitario di Scienze e Tecnologia dei Materiali, Via San Giusti 9, 50121, Firenze, Italy

[c] Dipartimento di Chimica, Università degli Studi di Pavia, Viale Taramelli 13, 27100, Pavia, Italy

[d] King Abdullah University of Science and Technology (KAUST), Biological and Environmental Sciences and Engineering (BESE) Division, NABLA Lab, 23955-6900 Thuwal, Saudi Arabia

† Current address: STMicroelectronics, Via Camillo Olivetti, 2, 20864 Agrate Brianza, Italy

* Corresponding Author. alessandro.minguzzi@unimi.it

Abstract

In this work we studied the kinetics of oxide formation and reduction on Pt nanoparticles in $HClO_4$ in the absence and in the presence of Br^- and Cl^- ions. The study combines potential step methods (i.e. chronoamperometry and choronocoulometry) with energy dispersive X-ray absorption spectroscopy (ED-XAS), which in principle allows to record a complete XAS spectrum in the timescale of milliseconds. Here, the information on the charge state and on the atomic surrounding of the considered element provided by XAS was exploited to monitor the degree of occupancy of 5*d* states of Pt in the course of oxide formation and growth, and to elucidate the competing halide adsorption/desorption phenomena. Electrochemical methods and XAS agree on the validity of a log(*t*) depending growth of Pt oxide, that is significantly delayed in the presence of Cl^- and Br^- anions. In the proximity of formation of one monolayer, the growth is further slowed down.

Keywords: time resolved XAS, spectroelectrochemistry, platinum oxidation, specific adsorption, chlorides, bromides.

1. Introduction

In this work we adopt operando energy dispersive X-ray absorption spectroscopy (ED-XAS) to study the effect of specifically adsorbing ions, namely Br^- and Cl^-, on the dynamics of Pt oxide growth. The aim is to couple the potentialities of electrochemical methods and of ED-XAS to trace a detailed dynamic picture of electrochemical phenomena in real time. In fact, ED-XAS is based on the use of a curved crystal "polychromator" that disperses X-ray energies and focuses them onto a focal plane that coincides with the sample (in the present case, the working electrode). The transmitted beam hits a position sensitive detector that records the intensities relevant to small intervals of energies.

Provided that the sample presents a sufficiently high surface-to-bulk atomic ratio (such as in small nanoparticles, or in "bulk active" materials [1]), the two techniques focus on the system synchronously, a crucial feature to detect the effect of adsorbed species on the kinetics of heterogeneous reactions, and specifically electrochemical charge-transfer reactions.

In this wide context, the most studied electrode material, for fundamental and application goals, is certainly platinum under both metallic and oxide forms, pure and in admixture with other elements.

For these reasons, the study of adsorbed species and of competitive adsorption on Pt is of paramount importance because of their implications in the operation of devices such as fuel cells and water electrolyzers. For example, the activity of Pt for the oxygen reduction reaction:

$$O_2 + 4e^- + 4H^+ \rightarrow 2H_2O \qquad (1)$$

is significantly hindered in the presence of sulfate ions (from Nafion® decomposition)[2]. In addition, the adsorption of oxygen species on Pt has been proposed as the reason behind the poor activity of Pt by blocking active sites and thus the first reaction step of the ORR, as it was demonstrated in single crystal electrodes [3]:

$$Pt\text{-}O_2 + e^- \rightarrow Pt\text{-}O_2^- \qquad (2)$$

~~Competition a~~ Adsorption phenomena can also hinder the desired reaction because of competition with the adsorption of the reagent. One of the most studied cases deals with fuel cell and Pt as the model electrocatalyst for both the oxygen reduction reaction (ORR, reaction (1)) and the hydrogen oxidation reaction (HOR):

$$H_2 \rightarrow 2H^+ + 2e^- \quad (3)$$

In the case of Pt, specifically adsorbed anions makes the ORR to proceed through a $n < 4e^-$ reduction pathway, as observed on Pt(111) [4].

On these bases, an intense research work has been dedicated to the problem of competitive adsorption between oxygenated species (OH, O, OOH) and anions.

The system is of particular complexity and the study of Pt oxidation itself has been at the basis of literature works since the early 70s' [5,6] and is still under investigation, also by means of sophisticated techniques, including synchrotron light-based ones [7–11].

A summary of the phenomena leading to the formation of PtOx starts from the existence of an "incipient oxide", in some cases observed even at open circuit, but with very low coverages[12].

At $E > 0.6$ V (RHE), adsorption of –OH or –O occurs and this likely implies a charge transfer from Pt.

At higher potentials, the so-called "place exchange" occurs (from coverage values higher than 0.5 [12]), where Pt and O positions shift in place and serves as the beginning of the growth of an "irreversible" oxide. Further increasing the applied potential, the "bulk" oxidation of Pt begins up to the limit case of PtO_2. Note that the formation of a place exchange between Pt and O has been recently verified by operando X-ray diffraction on Pt(111) [7].

The growth of Pt oxide proceeds through a series of steps that can include the (proton coupled) interfacial electron transfer, the place exchange of Pt and O in the structure, the diffusion within the growing oxide layer, the extraction of a metal ion at an interface. According to the two most considered models, the rate determining step is either the interfacial place exchange or the extraction of a metal cation. In the first case, a "direct" linear dependence of the integrated quantity of charge Q (and thus of oxidized Pt) on $\log(t)$ is observed [13], while, in the second one, Q^{-1} linearly depends on $\log(t)$ [14]: the "inverse"-logarithm growth. The two cases have been recently reconsidered to model the system [15] as a basis for DFT calculations [11]. In addition, it has been reported that the growth of PtO is limited to a few layers [16,17], while PtO_2 growth with no limits.

This complex behavior might be further complicated by the presence of competing specifically adsorbed (an)ions.

Many studies faced the problem of competitive adsorption of oxygen species and halides, from the earlier studies of Breiter and Bagotzky [18,19] to the works of Conway [20], who determined the % of blocked oxide as a function of Cl^-, Br^- and I^- concentration. More recently, the problem has been approached with XAS ([21,22]), to demonstrate the dependence on coverage of the –OH and –O adsorption sites and the effect of halide adsorption (in terms of weakening of Pt-Pt bonds and change of nanoparticle shapes) and competition.

Due to the particular complexity of the system, we believe that a spectroelectrochemical approach could help in better understanding the mechanism of the process while studying the time dependence of these phenomena. On these bases, we carried out a series of operando XAS experiments devoted to explore the time dependence of Pt oxidation in the absence and in the presence of Br^- and Cl^-. This type of investigation has never appeared in the scientific literature: ED-XAS has in fact been rarely used to study electrochemical phenomena. The existing literature limits to the study of Pt oxidation [8,13,23–25], Cu electro-dissolution [26], hydride and deuteride formation in Pd/C electrodes [27], redox properties of Ni hydroxide [28], the stability of a Cu complex [29] and charge transfers in hydrous Ir oxide films [30]. Since the very first experiments [13,23,24], the study of Pt oxide growth revealed its complexity, and the effectiveness of ED-XAS in studying it. In addition, most studies on metal oxides growth are relevant to polycrystalline, “massive” electrodes, whereas deep investigations (particularly fundamental ones) on nanoparticles are more scarce and require further attention mainly because of their (i) strong size-dependent activity[31][32][33], (ii) evident effect of the support [34] and (iii) synthetic method-dependent exposure of {h k l} facets [35].

2. Experimental

All solutions were prepared using MilliQ grade water. All reagents were purchased from Aldrich and used as received. The declared content of Cl^- ions in $HClO_4$ (ACS reagent, 70%) is of ≤0.001%. Pt nanoparticles deposited onto Vulcan XC72 R, Cabot, (Pt/C NPs) were kindly supplied by Industrie De Nora S.p.A. The Pt load onto carbon is 28.6 wt%.

2.1. Transmission Electron Microscopy. Pt/C NPs were characterized by high resolution transmission electron microscopy (HRTEM), X-ray diffraction (XRD). For HRTEM, a small drop of isopropanol in which the NPs were previously dispersed was deposited on an ultrathin carbon membrane mounted on a 400-mesh copper grid. Once the solvent was totally evaporated, HRTEM imaging was performed by an FEI Titan Cube 80-300kV microscope (Hillsboro, OR, USA), operating at an acceleration voltage of 300 kV, and equipped with an ultrabright X-FEG Schottky electron source, a spherical aberration corrector of the objective lens and a 2k × 2k US1000 Gatan CCD Camera, with an ultimate resolution of 0.8 Å.. The NP mean size (2 nm) obtained from HRTEM imaging was determined measuring more than one hundred nanoparticles using ImageJ software. Local analysis of the NPs crystal structure was then performed by Fourier Analysis of the HRTEM images, i.e. extracting the filtered bidimensional Fast Fourier Transform (2D-FFT), the latter being also called numerical electron diffraction pattern.
XRD analysis was performed on films obtained by evaporating 500 µL of the Pt/C NPs suspension on glass microscope slides with an area of ~2.2 cm^2. The XRD patterns were acquired using a Bruker D8 Advance diffractometer (Bruker Corp., Billerica, MA, USA) with a Cu anticathode (λ-Cu-Kα = 1.541838 Å) operating at 40 kV and 40 mA. Diffractograms were acquired in θ–θ mode, with a step of 0.02° 2θ and an acquisition time of 20 s per step. Phase indexing, determination of lattice constants, and average grain sizes have been performed using the HighScore Plus software from PANalytical. Application of the Sherrer equation gives a size of the crystallites equal to 3 nm, in good agreement with HRTEM determination.

2.2. Electrode preparation. Working electrodes were prepared by depositing 50 µL of 6 mg mL^{-1} of Pt/C NPs aqueous suspension (previously sonicated for 10 min) onto 1x1 cm^2 glassy carbon plates (Goodfellow). The suspension was deposited in three subsequent aliquots of 20 µL +20 µL +10 µL, with the electrode support on a hot plate (about 80°C). Finally, 2.5 µL of a 5.5% Nafion dispersion in isopropanol were added to guarantee powder adhesion.

2.3. Spectroelectrochemical cell. All preliminary Cyclic Voltammetries (CV), electrode materials conditioning and operando XAS experiments were carried out in a three-electrode cell in aqueous 0.1 M $HClO_4$. In selected experiments, 10 mM KBr or KCl were added to the $HClO_4$ electrolyte. The counter electrode (CE) consisted on platinum black deposited onto a platinum disk that faces the working electrode. The CE disk presented a central hole to allow for the passage of the X-ray beam. The reference electrode, a AgCl/Ag (KCl 1M) was in contact with the solution via a salt bridge, consisting in a glass pipette filled with agar and containing 0.2M aqueous $KClO_4$. The cell, that is schematically represented in Figure 1, consists of a polytetrafluoroethylene (PTFE) cylinder that presents a cylindrical, blind hole. The area of the hole, 0.78 cm^2 coincides with the exposed area of the working electrode. The latter is held in place between the cell and a PTFE ring that includes a hole for the X-Rays beam.

All electrochemical operando XAS experiments were carried out using a CH Instrument 633D potentiostat, driven by the proprietary software.

All potentials are referred to the reversible hydrogen electrode (RHE) electrode.

2.4. Operando Energy Dispersive - X-ray Absorption Spectroscopy. EDXAS data were collected at ID24 beam-line [36,37] of the European Synchrotron Radiation Facility, ESRF, Grenoble (the ring energy was 6.0 GeV and the current 150–200 mA). Spectra were recorded in transmission mode using a FReLoN (Fast Readout Low Noise) high frame rate detector [38]. The energy calibration was made by measuring the absorption spectrum of a Pt foil (Pt L_{III}: edge).

In operando XAS experiments, and particularly in energy dispersive XAS, when a high photon flux is considered, beam damage might represent a critical issue. Our strategy consisted in checking the spectra quality and consistency after each run and, in case of evident sample damage (e.g. poor spectra quality or significant loss of absorption), pointing the X-ray beam onto a different area of the sample. This is allowed by the small beam size (1×2 μm^2) compared to the electrode geometric surface area (0.2 cm^2).

In all cases, spectra recorded on different spots, at constant conditions, were superimposable, and the relative variations in the intensity of the transmitted beam with position in the sample were of the order of 10 %. The choice of the best beam position on the sample follows a rapid evaluation of X-ray absorption~~/oxide growth~~ from Pt over the entire sample area by means of a rapid 2D screening. Preferential impinging spots clearly coincide with points with higher Pt content.

Sequences of spectra were acquired while applying to the working electrode selected potential steps and recording the relevant chronoamperometries. Usually, oxidative and reductive potential steps were

coupled in sequence. In all cases, the working electrode was kept at the initial potential for about 2 minutes to allow initial stationary conditions. During this period, XAS spectra relevant to the initial condition were recorded for 2 s before the potential was set to its final value. The potential step was triggered by the XAS acquisition system. All measurements were carried out at room temperature. A sequence was made of 1000 spectra acquired every 50 ms. Averages were calculated every 10 spectra in order to obtain a better signal to noise ratio: this gives a final time resolution of 0.5 s. The raw XAS spectral data were processed with a preliminary stage, in which spectra were normalized, and a subsequent analysis aimed at extracting parameters for characterizing the time dependence of the involved processes. In the preliminary stage, each XAS spectrum of each sequence was normalized by means of the PRESTO PRONTO software [39], consisting of a full GUI EXAFS program aimed to the analysis of large data sets. Thanks to this software, it is possible to perform classical analysis, from the extraction to the EXAFS fit, of data coming from QEXAFS and DISPERSIVE beamlines. The normalization was made by (i) fitting the pre edge and post edge parts of the spectrum with a straight line or a cubic function and (ii) rescaling the whole spectrum to unit step in the absorption coefficient at the edge. The same pre edge fitting function was used for all spectra of a sequence, and analogously for the post edge fit. The XANES were then fitted by a Lorentzian plus arctangent function [40]. The area, *A*, of the Lorentzian peak was then used to calculate the Degree of Reaction (DoR) according to the equation:

$$DoR_{XAS} = \frac{[A_t]-[A_{t_0}]}{[A_{t_f}]-[A_{t_0}]} \quad (4)$$

3. Results and discussion.

Figure 2 shows a HRTEM image of Pt/C NPs (a). In (b) a selected NP, representative of the NPs ensemble, is shown at higher magnification, highlighting the single-crystalline structure, confirmed by the numerical electron diffraction pattern. Only the main lattice planes are indicated, in the insets, to preserve readability, and the numerical electron diffraction pattern displayed in panel (c) provides a further indication about crystal structure and orientation (being the zone axiz the [011]) of the particle imaged in panel (b).

The main lattice planes and indexing in Figure 2c show that the zone axis is [011] and Figure 2d shows the X-ray powder diffraction pattern, where the indexing refers to the FCC structure of metallic Pt.

HRTEM indicates that in Pt nanoparticles the {100} and {111} facets are exposed, and both XRPD and HRTEM point toward a crystal size of *ca.* 2-3 nm.

As described in the Experimental, Pt/C NPs were deposited onto glassy carbon electrodes, used as working electrodes. Before XAS experiments, the particles were pre-conditioned by fast cyclic voltammetry (1V s^{-1}) for 500 cycles between -0.2 and 1.6 V vs the reversible hydrogen electrode (RHE) in the same electrolyte used for the subsequent spectro-electrochemical experiment. This guarantees a clean and stable electrode surface at the starting conditions. On the other hand, the cleaning procedure can cause a dissolution of Pt at the highest potentials and re-deposition at the lowest leading to a partial reconstruction/sintering of NPs.

3.1. Experiments in 0.1 M $HClO_4$

As reference condition for the investigation of adsorption of oxygenated species on Pt nanoparticles we used aqueous 0.1 M $HClO_4$. ClO_4^- is usually assumed to have zero or negligible adsorption on Pt surfaces. However, recent studies showed that perchlorate anions can specifically adsorb on the Pt{111} surface, but this effect is almost insignificant on the Pt{100} surface [41]. Given that: i) the NPs investigated in this work present both surfaces exposed, and ii) the specific adsorption of ClO_4^- on the Pt{111} surface is relevant only at higher perchlorate concentrations (≥ 0.5 M [41]), we can assume that the 0.1 M $HClO_4$ solution is an adequate approximation of the condition of no specific adsorption. Correspondingly, Figure 3a shows the cyclic voltammetry of the Pt NPs at s 10 mV s^{-1} scan rate in this solution. This CV allows to safely identify two potential values: at 0.5 V vs the reversible hydrogen electrode (RHE) the Pt NPs are uncovered by oxygen species; on the contrary, at 1.4 V the adsorption process should reach the equivalent of 0.7-1 monolayers [12] and corresponds to the potential region where place exchange oxide is formed.

Therefore, our experimental approach consists in applying potential steps from 0.5 to 1.4 V and vice versa, and concomitantly recording the relevant current (sampling interval 1ms) and successive XAS spectra (one every 50 ms). As mentioned, 10 ED-XAS spectra are averaged with a final resolution of 0.5s. Figure 3b shows one of the Pt L_{III}-edge XANES spectra for the NPs, and Figures 3c-d and 3e-f show the time evolution of these spectra for the 0.5-1.4 V and 1.4-0.5 V potential steps, respectively. It is worth noting that the spectra recorded at 0.5 V at the start of the 0.5 – 1.4 V and end of the 1.4– 0.5 V sequences are completely superimposable to that of a standard Pt foil. The Pt L_{III}-edge XANES can be described as constituted by two main spectral features: a lorentzian peak, also called white line (WL),

that is due to transitions from Pt 2*p* to 5*d* states, and an arctangent step, that is due to the expulsion of a photoelectron from the Pt 2*p* states. It is quite apparent that an oxidation step in the considered interval (0.5 -1.4 V) causes an increase in the amplitude in the WL, due to an increase in the density of empty states in the Pt 5*d* band [42]. The intensity of the WL then decreases correspondingly after the reduction step (1.4-0.5 V). As described in the Experimental section, the XANES peak of each spectrum is fitted by a Lorentzian function and the peak amplitude is extracted; finally, the Degree of Reaction (DoR_{XAS}) is calculated.

Temporal sequences such as those reported in Figure 3c and 3e evidence that the WL amplitude ceases to significantly change after 4-5 s. Thus, after 5 s the DoR_{XAS} was set to 1. The integrated areas and relevant DoR values for the growth and reduction of Pt oxide are shown in Fig. 4a and 4b, respectively. It is readily seen that both processes are quite fast and are almost completed within the first 4-5 seconds, the desorption being apparently slightly faster.

Figure 4c reports the chronoamperometric response of the electrode in 0.1M $HClO_4$ as recorded during XAS spectra acquisition. Here, *I*/*t* curves are reported together with the relevant integrated quantities of charge (*Q*). A direct and quantitative comparison between DoR_{XAS} and *Q* will be discussed below but we can immediately notice that chronoamperometry leads to considerations parallel to those indicated by XAS: the reduction of oxidized Pt is faster than its formation and both phenomena are almost complete after 2-3 seconds.

Note that all chronoamperometries reported in the present paper have been corrected for the contribution of double layer capacitance, whose current was calculated as follows:

$$I_{DL} = \frac{\Delta E}{R} e^{-\frac{t}{RC_{DL}}} \qquad (5)$$

Where I_{DL} is the current related to the charging of the double layer capacitance, ΔE the difference between the ending and starting potentials of the step, *R* the charge transport resistance, C_{DL} the double layer capacitance and *t* is time.

The values for *R* (40 to 48 Ohm) and C_{DL} (between 2 and 3 10^{-3} F) have been adjusted starting from data by impedance spectroscopy and cyclic voltammetry.

It is worth noting that we carried out additional experiments that considered potential steps up to 1.1 V RHE, which corresponds to an equivalent coverage of PtOH or PtO < 0.5 and just at the beginning of the "place-exchange" oxide region [12]. Nonetheless, this choice did not lead to any modification of the

XANES peak area. This is likely due to the too low effect onto Pt 5*d* orbitals by the partial OH or O coverage that remains indistinguishable from interface water.

3.2. Experiments in the presence of Cl^- and Br^-

When the experiments are repeated in the presence of Cl^- and Br^- 10 mM, the results are strikingly different.

This is well evident in Figure 5 that reports CVs recorded in the presence of the two halides, which shift Pt oxidation/reduction characteristics [43].

Figures 5 b and c compare DoR_{XAS} to the normalized quantity of charge, Q/Q_f, where Q is the quantity of charge obtained by integration up to time t, and Q_f is the total quantity of charge, observed up to the final time, t_f. In this case, temporal sequences of spectra (not shown) evidence that the WL amplitude ceases to significantly change after about 20s. The CVs (Fig. 5a) support that in the 0.5 – 1.4 V potential step oxygenated species are adsorbed and the PtO grows, thus allowing to study the competition with Cl^- and Br^-, which are expected to be adsorbed already at 0.5 V [44–47]. In particular: i) both halides slow down the rate of the Pt oxidation/reduction processes; ii) the oxidation process is slower than the reduction one, and iii) Br^- has a larger influence than Cl^- on the overall kinetics. These findings can be easily explained noting that at 0.5 V both the halides are specifically adsorbed, acting then as blocking species for the adsorption of oxygenated species: the effect of Br^- is larger than that of Cl^-, likely due to the larger size of bromide. Size is strictly related to polarizability [48] and thus to adsorption energy.

It should also be noted that the WL amplitude at the end of the oxidation process is not dependent on the nature of the halide or even on their presence. This indicates that the thickness of the oxide layer is the same in the three cases investigated in this work.

To estimate the effect of the halide ions on the rate of the Pt oxidation/reduction processes, a "delay time", t_d is defined as the half-life (by DoR) in the current conditions normalized by the corresponding half-life as measured in 0.1 M $HClO_4$. The results are shown in Table 1.

Table 1. Adimensional delay time, t_d.

	t_d	
	0.5 → 1.4 V	1.4 → 0.5 V
Cl^-	4.55 ± 0.01	2.62 ± 0.01
Br^-	4.78 ± 0.01	2.78 ± 0.01

Table 1 evidences that the delay related to the presence of Cl^- and Br^- ions is, as can be expected, much higher for the oxide formation than for its stripping. About the latter phenomenon, one can be surprised for the actual evidence of a delay. It has to be noted, though, that this reflects the differences of the Pt oxide reduction peak potential that are evident from figure 5a (where potentials in the abscissa are corrected for *IR* drops). As a possible explanation, earlier works [43] suggest that halides remain, at least partially, adsorbed on the forming oxide. This could in turn cause a delay also in the reduction process.

From Figure 5, it is readily seen that Q/Q_f and DoR_{XAS} show a nice agreement for all experiments. Note that, for the reasons mentioned earlier, the condition for $DoR_{XAS}=1$ does not represent the complete oxidation of Pt NPs. Still, the timescale of the phenomena detected by the current is apparently different from that detected by XAS. In particular, while in all cases the DoR_{XAS} reaches unit values within 3-10 s at maximum, Q/Q_f requires several tens of seconds for reaching a saturation value.

These evidences point towards the fact that Q/Q_f might detect additional phenomena compared to DoR_{XAS}. For example, the outcomes of the present investigation will be crucial in future investigation where the ORR will occur in parallel to Pt oxide growth/reduction. In addition, it has to be pointed out that XAS data are relevant to the occupancy of Pt *5d* orbitals, whereas O, Cl and Br *p* ones likely contribute to the phenomena involved in the present investigation and thus to integrated quantities of charge. This aspect represents one of the main advantages of combining electrochemical methods with X-ray spectroscopies, which allows decoupling parallel electrochemical phenomena and to address specific electronic information.

For what concerns the analysis of Q and DoR as a function of t, the oxidation step (i.e. the Pt oxide growth) deserves particular attention. In fact, Figure 6a evidences that there is a linear dependence of both Q/Q_f and DoR_{XAS} on $\log(t)$, as earlier observed by Conway [49] and in following reports [16,25]. On the contrary, any model for an "inverse"-logarithm growth cannot be applied in the present case, as shown in Figure 6b.

In both cases, the small discrepancies between Q/Q_f and DoR_{XAS} at small t can reflect the already mentioned selectivity of XAS in addressing solely the occupancy of Pt *5d* orbitals.

Now, it is of particular interest to further discuss the experimental results with respect to a "direct" logarithm oxide growth. As can be observed from Figure 6a, the linear growth starts, in all cases, after about $\log(t)=0$ (1s). This could be due to the initial formation of Pt-OH [10,50,51], even though some experimental evidence points to the conclusion that Pt oxidation proceeds directly to PtO and without OH_{ads} as an intermediate [16]. In addition, we can rule out the formation of PtO_2, as well as of the

complete transformation of Pt nanoparticles into PtO. In fact, comparing the loading of Pt on the electrode with Q_f, we can conclude that about 50 % of Pt underwent oxidation to PtO after a full oxidation step.
In the presence of halides, the initial non-linear trend is likely related to the need of displacing/substituting the already present competing anions.
Another interesting aspect of growth curves is the evident change of slope in Figure 6a. This occurs in $HClO_4$ at about log(t)=0.5 for both DOR_{XAS} and Q/Q_f. However, in the presence of the halides, a visible change in slope is apparent at log(t)=1.2 only for Q/Q_f, at the time at which DoR_{XAS} reaches unity. Now we assign θ_{OX} = 1 (1 monolayer) at $Q_{OX} = 2Q_H$ (formally PtO)[12] where Q_H corresponds to the quantity of charge due to hydrogen adsorption/desorption, determined by averaging the anodic and cathodic areas of the CV shown in Figure 3a. In 0.1 M $HClO_4$, $Q_{OX}/Q_f \approx 0.8$, which corresponds to the slope change of Q/Q_f vs log(t) plots in all solutions as well as to the appearance of a divergence between DoR_{XAS} and Q/Q_f in the presence of the halides. On these bases, we can conclude that the two linear sections in the DoR_{XAS} and Q/Q_f vs log(t) are separated by the oxidation of the first monolayer of Pt NPs. This in turn means that the reaction rate slows down after the first monolayer of PtO is formed and the rate determining step changes. This occurs irrespective from the presence of halides, which affect primarily the formation of the first PtO monolayer. The following dramatic decrease of rate could be at the basis of the apparent end of the reaction by the "eye" of XAS: the oxidation of Pt after the initial few seconds is too slow to be quantified by the XANES peak area, within the experimental error.
In fact, the current intensity I, i.e. the rate of reaction, shows an initial value 10 times higher than that at Q/Q_f >0.8.
This is in agreement with the information given by XAS spectra: Figure 7 compares single XAS spectra recorded during the reaction with standard Pt and PtO. It is evident that, for DoR_{XAS} = 1, the deposit (blue and green lines) is far from being fully oxidized to PtO. In fact, the oxidized deposit is quite comparable to a simulated spectrum, reported as a pink, dashed line, generated by a linear combination of the Pt and PtO standard spectra, applying a spectral weight of 50:50.

4. Conclusions

In this work we adopted operando energy dispersive X-ray absorption spectroscopy to the study of Pt oxide growth in 0.1M $HClO_4$ (assuming ClO_4^- as a non-adsorbing ion) and in the presence of halide ions, Br^- and Cl^-.

The setup allows to record chronoamperometries relevant to a pre-defined potential step and to parallel record XANES spectra (one every 50 ms). This allows in turn to monitor the occupancy of Pt 5 *d* states and to evaluate the composition of the electrode while the electrochemical reaction occurs.

Here the Pt oxide growth was stimulated by a 0.5-1.4 V (RHE) potential step. In all solutions, the expected Q vs $\log(t)$ linearity is satisfied but, in the presence of halide ions, the kinetics is significantly more sluggish. This effect is more evident for Br^- ions, likely due to their higher polarizability.

Noteworthy, a partial discrepancy between DoR_{XAS} and Q/Q_f at low $\log(t)$ might point to the fact that the first selectively reflects any change of occupancy of Pt *d* states, while the second is non-selective in this sense. This could be explained by an active role played by O, Br and Cl during adsorption, where anions are redox active, as observed in Li-ion batteries[52]. However, further experiments are needed to confirm this hypothesis, which would strengthen the interesting complementarity between the two techniques.

After a quantity of charge close to the one needed to form one monolayer of PtO, the slope of Q vs $\log(t)$ decreases and the degree of reaction calculated from XAS spectra analysis reaches 1. This is possibly due to the fact that the formation of the first monolayer occurs quite rapidly, but the place exchange of Pt and O needed to deepen the PtO formation slows the reaction, as witnessed by I, the latter being one order of magnitude than at t=0. At the end of the step, about half of the deposited Pt is oxidized, as confirmed by the analysis of XANES spectra.

These outcomes confirm those obtained by Zolfaghari, Conway and Jerkiewicz [43], who observed the existence of two stages in the formation of Pt oxide and that the blocking effect by Cl^- and Br^- occurs mainly in the first one. In the present work we aimed at studying Pt nanoparticles, whose morphologic and electronic features deeply alter the final electrode behavior in comparison to massive single-polycrystalline electrodes. This is particularly evident considering adsorption energies [53], which have a deep impact on oxide growth and stripping, in the absence and presence of specifically adsorbing ions.

5. Acknowledgements

We are grateful to Industrie De Nora S.p.A. for having supplied Pt nanoparticles deposited on carbon.

The ESRF is kindly acknowledged for the provision of beamtime (Exp. CH-4951). We are grateful to Dr. Sara Morandi for her considerable help during data collection. We also acknowledge the ID24 beamline staff, and, in particular, Dr. Debora Motta Meira, for considerable help during data collection and analysis.

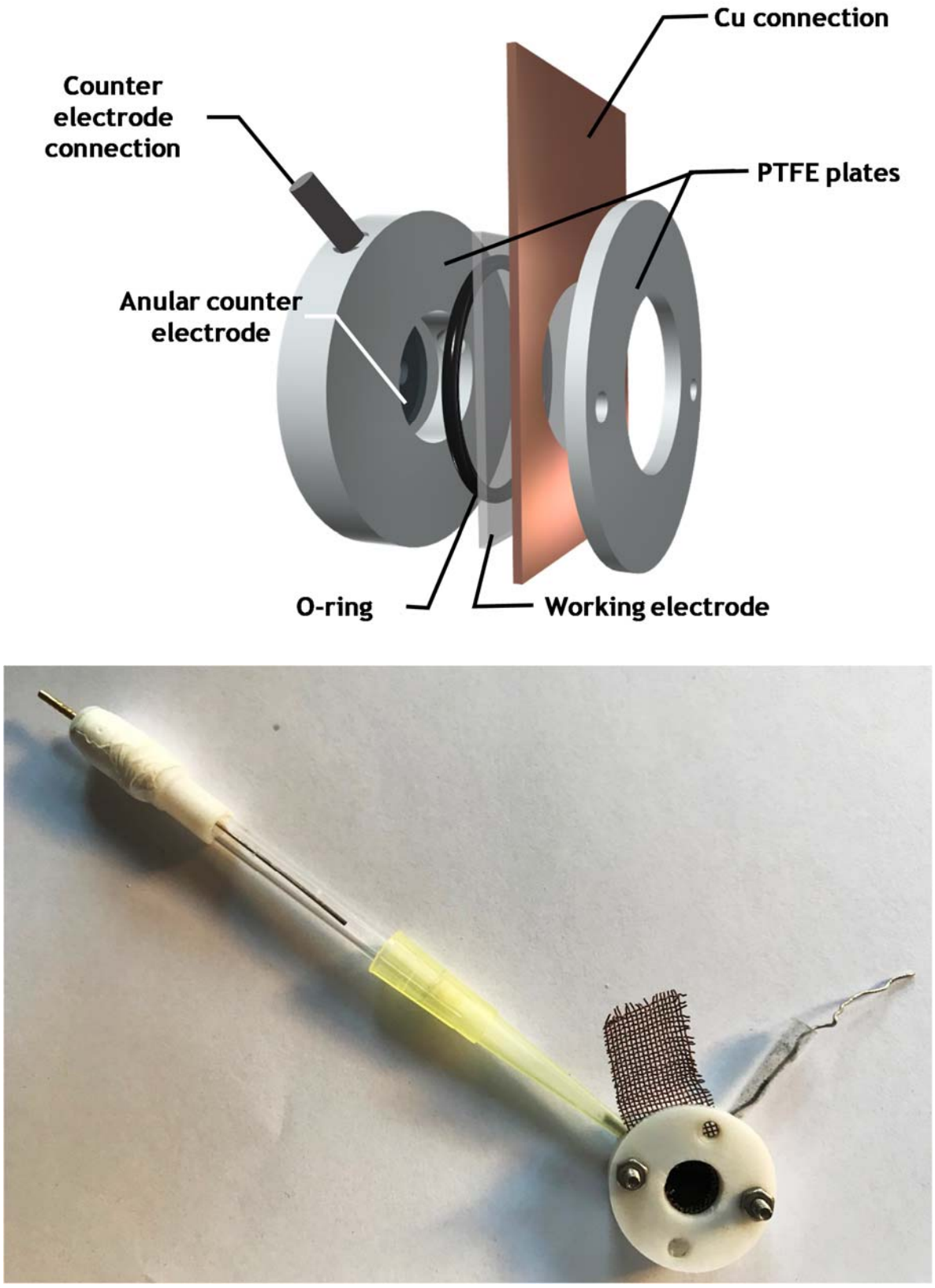

Figure 1. Schematic representation and picture of the spectroelectrochemical cell

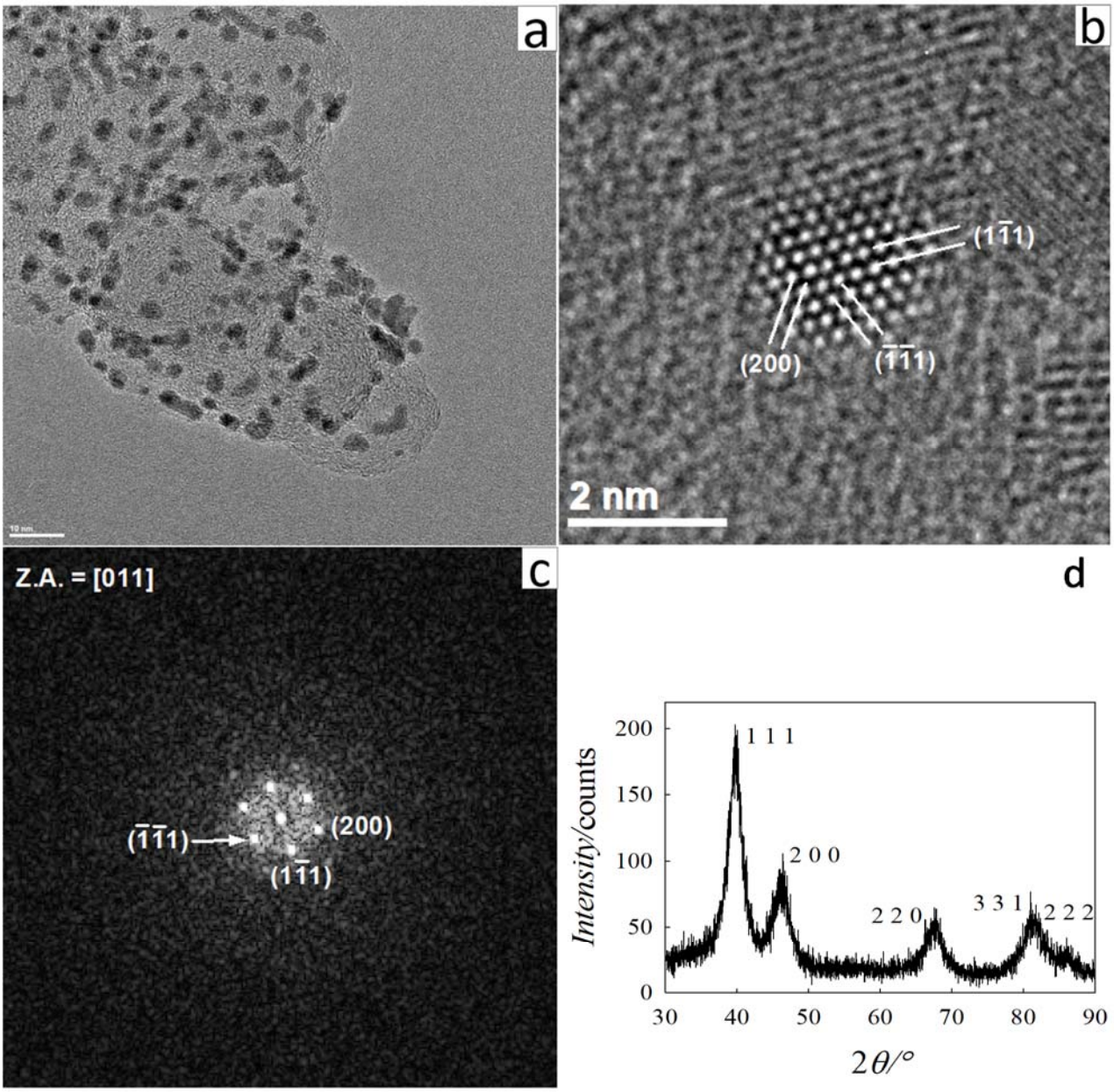

Figure 2. Characterization of the Pt NPs. (A) HRTEM images of representative CNPs. Magnified regions, shown in (B), highlight the single-crystalline FCC structure of Pt NPs, as also confirmed by the numerical electron diffraction pattern (filtered 2D-FFT) (C). The main lattice planes and indexing in (C) show that the particle zone axis is [011]. In (D) the X-ray powder diffraction pattern is shown. The indexing refers to the FCC structure of metallic Pt.

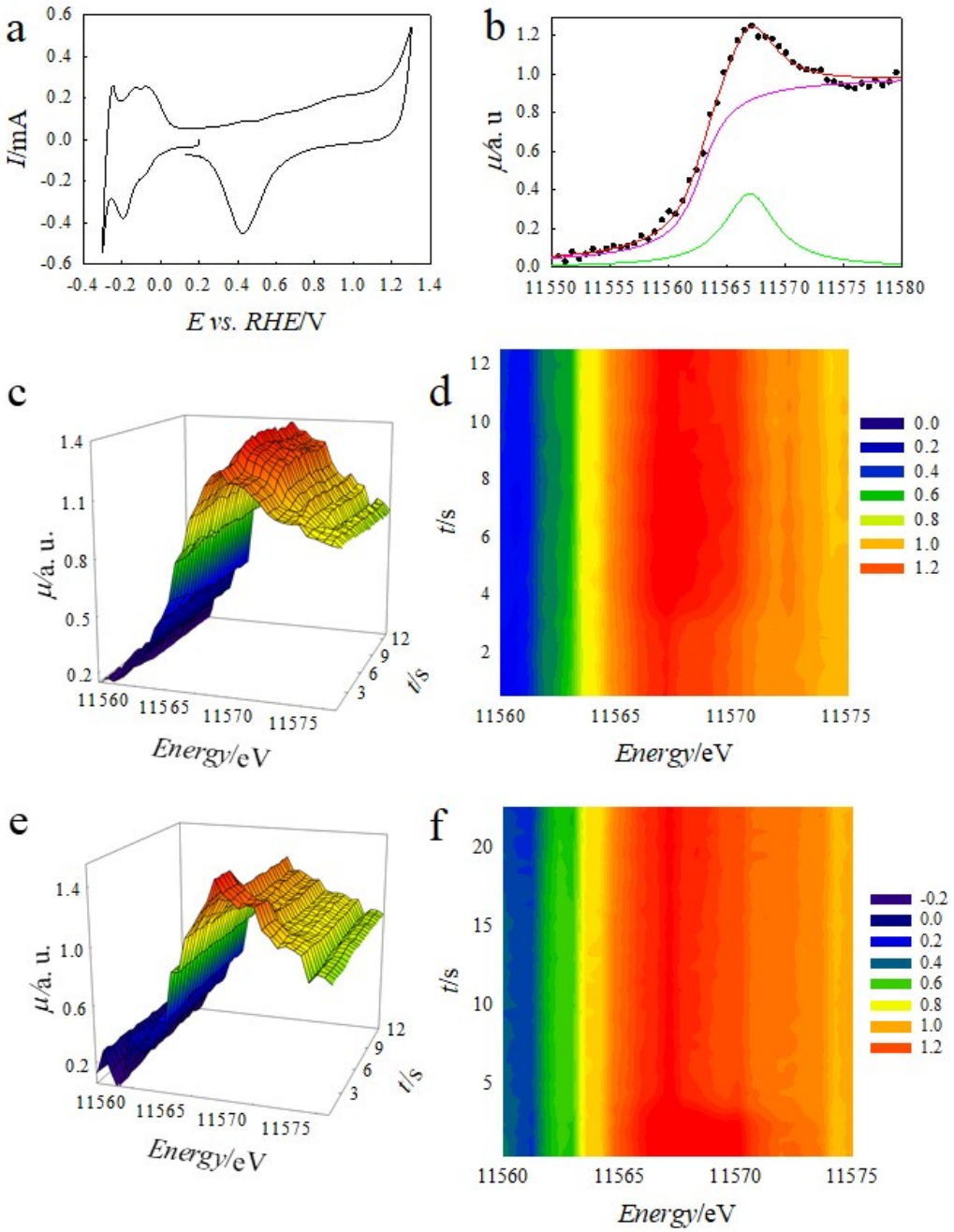

Figure 3. In (A) the Cyclic voltammetry of the Pt NPs in $HClO_4$ 0.1 M at 10 mV s^{-1}. The following panels show the EDXAS results at the Pt-L_{III} edge in $HClO_4$ 0.1 M. (B): a selected raw spectrum and fit according to the model described in the text. (C) and (E): color coded 3D images of the time evolution of the WL, for the (C): 0.5-1.4 V and (E): 1.4-0.5 V potential steps. In (D) and (F) the same plots are shown as contour maps.

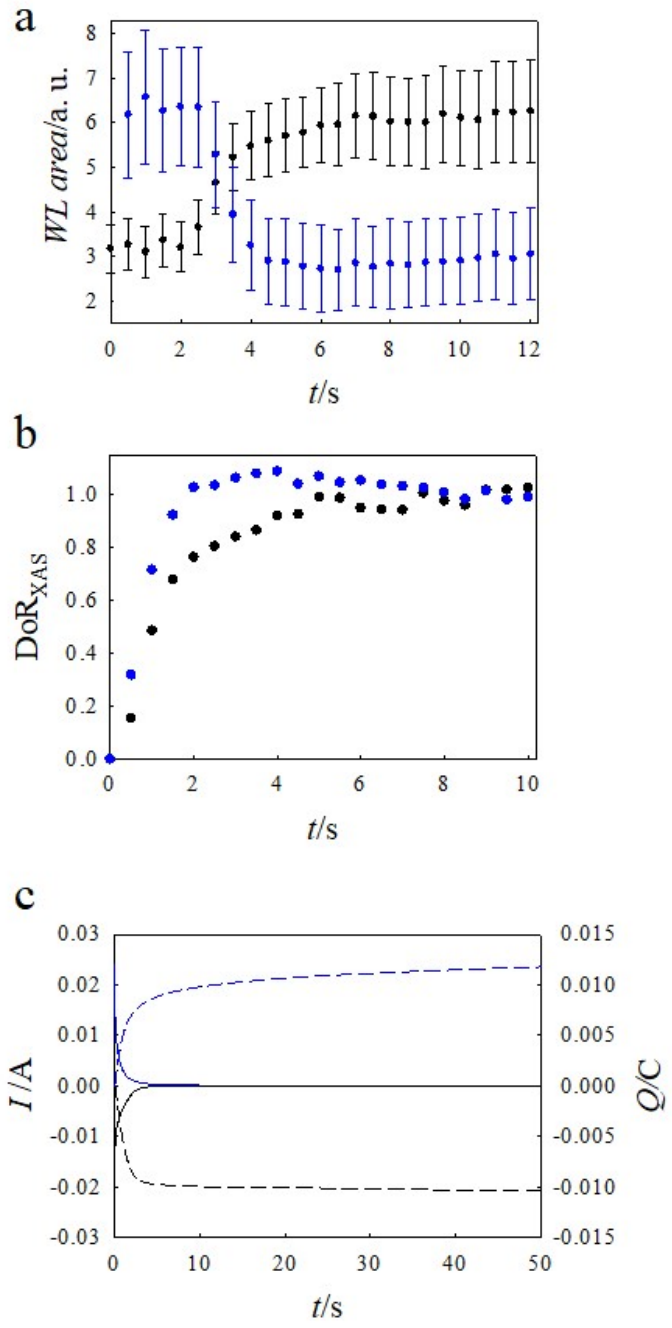

Figure 4. (A) white line amplitudes as derived from the fits shown in Fig. 2B (0.1M $HClO_4$) plotted as a function of time. The red line indicates when the potential step is applied. In (B) the corresponding degrees of reaction (DoRs) are shown. (C) Current (full lines) and integrated, cumulative quantities of charge (dashed lined). In all cases the 0.5 – 1.4 (blue dots) and 1.4 -0.5 (black dots) steps are shown.

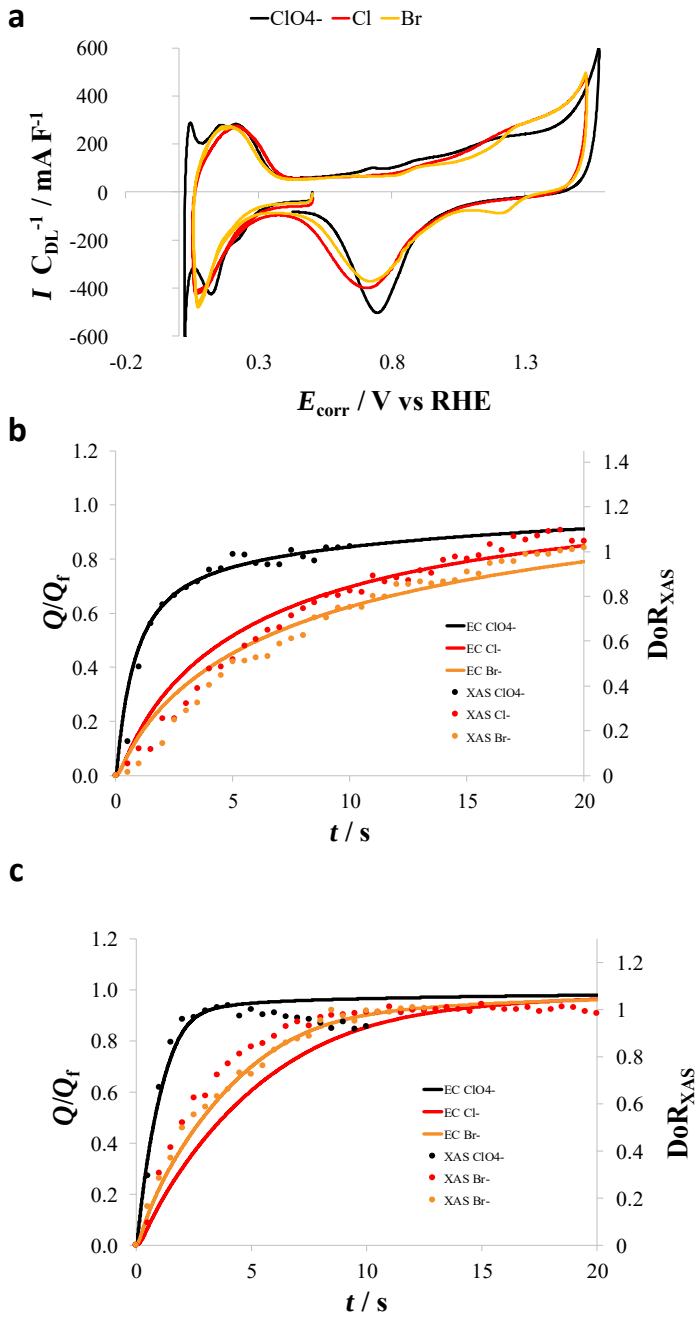

Figure 5. (a) *IR* corrected cyclic voltammetries recorded at 10 mV s^{-1}, (b) and (c) integrated quantities of charge, Q (normalized by the Q integrated at the end of the step, Q_f full lines) and DoR_{XAS} (dots): (b) 0.5 – 1.4 V and (c) 1.4 – 0.5 V potential steps. Black symbols: 0.1 M $HClO_4$, Red symbols: 0.1 M $HClO_4$ + 10 mM KCl, and Orange symbols 0.1 M $HClO_4$ + 10 mM KBr.

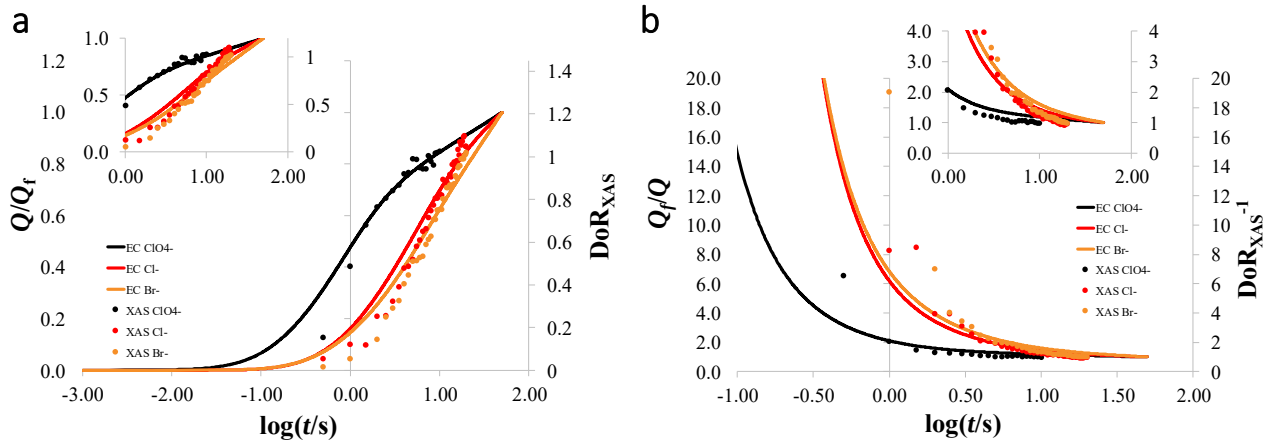

Figure 6. (a) Q/Q_f (full lines) and DoR_{XAS} (dots) and (b) $(Q/Q_f)^{-1}$ (full lines) and DoR_{XAS}^{-1} (dots) as a function of log(*t*) for the 0.5-1.4V step. In all figures, data recorded in 0.1 M $HClO_4$ (black), 0.1 M $HClO_4$ + 10 mM KCl (red) and 0.1 M $HClO_4$ + 10mM KBr (orange) are shown.

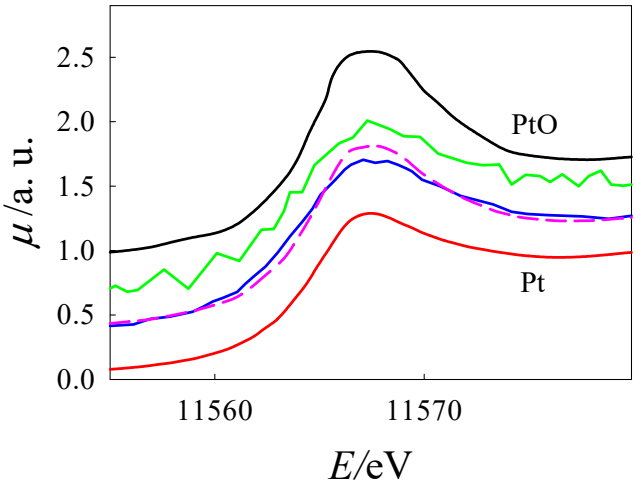

Figure 7. Comparison between the spectra of standard Pt (red line) and PtO (black line), and the final spectra of the sequence 0.2 – 1.1 V in $HClO_4$ (blue line) and $HClO_4$ + Cl^- (green line). The pink, dashed line represents a linear combination of Pt:PtO (standards) 50:50.

References

[1] P. Ghigna, A. Minguzzi, X-ray absorption spectroscopy in electrochemistry: from fundamentals to the fixed energy x-rays absorption voltammetry, in: Electroanal. Chem. a Ser. Adv. Vol. 27, 2017.

[2] H. Yano, T. Uematsu, J. Omura, M. Watanabe, H. Uchida, Effect of adsorption of sulfate anions on the activities for oxygen reduction reaction on Nafion Ò -coated Pt / carbon black catalysts at practical temperatures, 747 (2015) 91–96. doi:10.1016/j.jelechem.2015.04.007.

[3] V. Briega-martos, E. Herrero, J.M. Feliu, Electrochimica Acta Effect of pH and Water Structure on the Oxygen Reduction Reaction on platinum electrodes, Electrochim. Acta. 241 (2017) 497–509. doi:10.1016/j.electacta.2017.04.162.

[4] N.M. Markovic, H.A. Gasteiger, B.N. Grgur, P.N. Ross, Oxygen reduction reaction on Pt (lll): effects of bromide, J. Electroanal. Chem. 467 (1999) 157–163. doi:10.1016/S0022-0728(99)00020-0.

[5] K.J. Vetter, J.W. Schultze, THE KINETICS OF THE ELECTROCHEMICAL FORMATION AND REDUCTION OF MONOMOLECULAR OXIDE LAYERS ON PLATINUM IN 0.5 M H2S04, Electroanal. Chem. 34 (1972) 141–158.

[6] B.E. Conway, Electrochemical At Noble Metals Oxide Film Formation As a Surface-Chemical Process, Prog. Surf. Sci. 49 (1995) 331–452. doi:Doi 10.1016/0079-6816(95)00040-6.

[7] J. Drnec, M. Ruge, F. Reikowski, B. Rahn, F. Carlà, R. Felici, J. Stettner, O.M. Magnussen, D.A. Harrington, Initial stages of Pt(111) electrooxidation: dynamic and structural studies by surface X-ray diffraction, Electrochim. Acta. 224 (2017) 220–227. doi:10.1016/j.electacta.2016.12.028.

[8] O. Sekizawa, T. Uruga, K. Higashi, T. Kaneko, Y. Yoshida, T. Sakata, Y. Iwasawa, Simultaneous Operando Time-Resolved XAFS-XRD Measurements of a Pt/C Cathode Catalyst in Polymer Electrolyte Fuel Cell under Transient Potential Operations, ACS Sustain. Chem. Eng. 5 (2017) 3631–3636. doi:10.1021/acssuschemeng.7b00052.

[9] Y. Takagi, H. Wang, Y. Uemura, T. Nakamura, L. Yu, O. Sekizawa, T. Uruga, M. Tada, G. Samjeské, Y. Iwasawa, T. Yokoyama, In situ study of oxidation states of platinum nanoparticles on a polymer electrolyte fuel cell electrode by near ambient pressure hard X-ray photoelectron spectroscopy, Phys. Chem. Chem. Phys. 19 (2017) 6013–6021. doi:10.1039/C6CP06634H.

[10] Y.-F. Huang, P.J. Kooyman, M.T.M. Koper, Intermediate stages of electrochemical oxidation of single-crystalline platinum revealed by in situ Raman spectroscopy, Nat. Commun. 7 (2016)

12440. doi:10.1038/ncomms12440.

[11] M.J. Eslamibidgoli, M.H. Eikerling, Atomistic Mechanism of Pt Extraction at Oxidized Surfaces: Insights from DFT, Electrocatalysis. 7 (2016) 345–354. doi:10.1007/s12678-016-0313-2.

[12] J. Rodríguez-López, A. Minguzzi, A.J. Bard, Reaction of various reductants with oxide films on Pt electrodes As studied by the surface interrogation mode of scanning electrochemical microscopy (SI-SECM): Possible validity of a Marcus relationship, J. Phys. Chem. C. 114 (2010) 18645–18655.

[13] A. Dent, J. Evans, M. Newton, J. Corker, A. Russell, M.B. Abdul Rahman, S. Fiddy, R. Mathew, R. Farrow, G. Salvini, P. Atkinson, High-quality energy-dispersive XAFS on the 1 s timescale applied to electrochemical and catalyst systems., J. Synchrotron Radiat. 6 (1999) 381–383. doi:10.1107/S0909049599002150.

[14] N. Cabrera, N.F. Mott, Theory of the oxidation of metals, Reports Prog. Phys. 12 (1949) 308. doi:10.1088/0034-4885/12/1/308.

[15] H.A. Baroody, G. Jerkiewicz, M.H. Eikerling, Modelling oxide formation and growth on platinum, J. Chem. Phys. 146 (2017). doi:10.1063/1.4979121.

[16] M. Alsabet, M. Grden, G. Jerkiewicz, Comprehensive study of the growth of thin oxide layers on Pt electrodes under well-defined temperature, potential, and time conditions, J. Electroanal. Chem. 589 (2006) 120–127. doi:10.1016/j.jelechem.2006.01.022.

[17] G. Tremilios-Filho, G. Jerkiewicz, B.E. Conway, Characterization and Significance of the Sequence of Stages of Oxide Film Formation at Platinum Generated by Strong Anodic Polarization, Langmuir. 8 (1992) 658–667. doi:10.1021/la00038a059.

[18] M.W. Breiter, Voltammetric study of halide ion adsorption on platinum in perchloric acid solutions, Electrochim. Acta. 8 (1963) 925–935. doi:10.1016/0013-4686(62)87047-9.

[19] V.S. Bagotzky, Y.B. Vassilyev, J. Weber, J.N. Pirtskhalava, Adsorption of anions on smooth platinum electrodes, J. Electroanal. Chem. Interfacial Electrochem. 27 (1970) 31–46. doi:10.1016/S0022-0728(70)80200-5.

[20] D.M. Novak, B.E. Conway, Competitive adsorption and state of charge of halide ions in monolayer oxide film growth processes at Pt anodes, J. Chem. Soc. Faraday Trans. 1 Phys. Chem. Condens. Phases. 77 (1981) 2341–2359. doi:10.1039/f19817702341.

[21] T.M. Arruda, B. Shyam, J.M. Ziegelbauer, S. Mukerjee, D.E. Ramaker, Investigation into the competitive and site-specific nature of anion adsorption on Pt using in situ X-ray absorption

spectroscopy, J. Phys. Chem. C. 112 (2008) 18087–18097. doi:10.1021/jp8067359.

[22] M. Teliska, V.S. Murthi, S. Mukerjee, D.E. Ramaker, Site-specific vs specific adsorption of anions on Pt and Pt-based alloys, J. Phys. Chem. C. 111 (2007) 9267–9274. doi:10.1021/jp071106k.

[23] P.G. Allen, S.D. Conradson, M.S. Wilson, S. Gottesfeld, I. D.Raistrick, J. Valerio, M. Lovato, Direct observation of surface oxide formation and reduction on platinum clusters by time-resolved X-ray absorption spectroscopy, J. Electroanal. Chem. 384 (1995) 99–103.

[24] P.G. Allen, S.D. Conradson, M.S. Wilson, S. Gottesfeld, I.D. Raistrick, J. Valerio, M. Lovato, In situ structural characterization of a platinum electrocatalyst by dispersive x-ray absorption spectroscopy, Electrochim. Acta. 39 (1994) 2415–2418.

[25] H. Imai, K. Izumi, M. Matsumoto, Y. Kubo, K. Kato, Y. Imai, In Situ and Real-Time Monitoring of Oxide Growth in a Few Monolayers at Surfaces of Platinum Nanoparticles in Aqueous Media In Situ and Real-Time Monitoring of Oxide Growth in a Few Monolayers at Surfaces of Platinum Nanoparticles in Aqueous, J. Am. Chem. Soc. 131 (2009) 6293–6300. doi:10.1021/ja810036h.

[26] R. O'Malley, A. Vollmer, J. Lee, I. Harvey, J. Headspith, S. Diaz-Moreno, T. Rayment, Time-resolved studies of diffusion via energy dispersive X-ray absorption spectroscopy, Electrochem. Commun. 5 (2003) 1–5. http://www.sciencedirect.com/science/article/pii/S1388248102005167.

[27] A. Rose, O. South, I. Harvey, S. Diaz-Moreno, J.R. Owen, A.E. Russell, In situ time resolved studies of hydride and deuteride formation in Pd/C electrodes via energy dispersive X-ray absorption spectroscopy., Phys. Chem. Chem. Phys. 7 (2005) 366–372. doi:10.1039/b412066c.

[28] J. McBreen, W.E. O'Grady, G. Tourillon, E. Dartyge, a. Fontaine, K.I. Pandya, In situ time-resolved x-ray absorption near edge structure study of the nickel oxide electrode, J. Phys. Chem. 93 (1989) 6308–6311. doi:10.1021/j100354a010.

[29] E. Achilli, A. Vertova, A. Visibile, C. Locatelli, A. Minguzzi, S. Rondinini, P. Ghigna, Structure and Stability of a Copper(II) Lactate Complex in Alkaline Solution: A Case Study by Energy-Dispersive X-ray Absorption Spectroscopy, Inorg. Chem. 56 (2017). doi:10.1021/acs.inorgchem.7b00553.

[30] S. Rondinini, A. Minguzzi, E. Achilli, C. Locatelli, G. Agostini, G. Spinolo, A. Vertova, P. Ghigna, The dynamics of pseudocapacitive phenomena studied by Energy Dispersive XAS on hydrous iridium oxide electrodes in alkaline media, Electrochim. Acta. 212 (2016) 247–253. doi:10.1016/j.electacta.2016.06.149.

[31] K.J.J. Mayrhofer, B.B. Blizanac, M. Arenz, V.R. Stamenkovic, P.N. Ross, N.M. Markovic, The impact of geometric and surface electronic properties of Pt-catalysts on the particle size effect in electrocatalysis, J. Phys. Chem. B. 109 (2005) 14433–14440. doi:10.1021/jp051735z.

[32] S. Mukerjee, J. McBreen, Effect of particle size on the electrocatalysis by carbon-supported Pt electrocatalysts: an in situ XAS investigation, J. Electroanal. Chem. 448 (1998) 163–171. doi:10.1016/S0022-0728(97)00018-1.

[33] Y. Takasu, N. Ohashi, X.G. Zhang, Y. Murakami, H. Minagawa, S. Sato, K. Yahikozawa, Size effects of platinum particles on the electroreduction of oxygen, Electrochim. Acta. 41 (1996) 2595–2600. doi:10.1016/0013-4686(96)00081-3.

[34] A. Minguzzi, O. Lugaresi, G. Aricci, S. Rondinini, A. Vertova, Silver nanoparticles for hydrodehalogenation reduction: Evidence of a synergistic effect between catalyst and support, Electrochem. Commun. 22 (2012) 25–28. doi:10.1016/j.elecom.2012.05.014.

[35] C.M. Sa, F.J. Vidal-iglesias, A. Aldaz, V. Montiel, E. Herrero, Imaging Structure Sensitive Catalysis on Different Shape-Controlled Platinum Nanoparticles, (2010) 5622–5624.

[36] S. Pascarelli, O. Mathon, M. Muñoz, T. Mairs, J. Susini, Energy-dispersive absorption spectroscopy for hard-X-ray micro-XAS applications, J. Synchrotron Radiat. 13 (2006) 351–358. doi:10.1107/S0909049506026938.

[37] S. Pascarelli, O. Mathon, Advances in high brilliance energy dispersive X-ray absorption spectroscopy, Phys. Chem. Chem. Phys. 12 (2010) 5535–5546 |. doi:10.1039/b926434e.

[38] J.-C. Labiche, O. Mathon, S. Pascarelli, M.A. Newton, G.G. Ferre, C. Curfs, G.B.M. Vaughan, A. Homs, D.F. Carreiras, The fast readout low noise camera as a versatile x-ray detector for time resolved dispersive extended x-ray absorption fine structure and diffraction studies of dynamic problems in materials science, chemistry, and catalysis, Rev. Sci. Instrum. 78 (2007) 91301. doi:10.1063/1.2783112.

[39] S.J.A. Figueroa, C. Prestipino, PrestoPronto: a code devoted to handling large data sets, J. Phys. Conf. Ser. 712 (2016) 12012. doi:10.1088/1742-6596/712/1/012012.

[40] P. Ghigna, G. Spinolo, M. Scavini, U.A. Tamburini, A.V. Chadwick, The atomic and electronic structure of cerium substitutional defects in Nd2−xCexCuO4+δ An XAS study, Phys. C Supercond. 253 (1995) 147–155. doi:10.1016/0921-4534(95)00497-1.

[41] G.A. Attard, A. Brew, K. Hunter, J. Sharman, E. Wright, Specific adsorption of perchlorate anions on Pt{hkl} single crystal electrodes, Phys. Chem. Chem. Phys. 16 (2014) 13689–13698. doi:10.1039/C4CP00564C.

[42] M. Teliska, W.E. O'Grady, D.E. Ramaker, In situ determination of O (H) adsorption sites on Pt based alloy electrodes using X-ray Absorption Spectroscopy, J. Phys. Chem. B. 109 (2005) 8076–8084.

[43] A. Zolfaghari, B.E. Conway, G. Jerkiewicz, Elucidation of the effects of competitive adsorption of Cl-and Br- ions on the initial stages of Pt surface oxidation by means of electrochemical nanogravimetry, Electrochim. Acta. 47 (2002) 1173–1187. doi:10.1016/S0013-4686(01)00841-6.

[44] H.A. Gasteiger, N.M. Marković, P.N. Ross, Bromide Adsorption on Pt(111): Adsorption Isotherm and Electrosorption Valency Deduced from RRD Pt(111) E Measurements, Langmuir. 12 (1996) 1414–1418. doi:10.1021/la950826s.

[45] J.M. Orts, R. Gomez, J.M. OFeliu, Bromine monolayer adsorption on Pt (110) surfaces, J. Electroanal. Chem. 467 (1999) 11–19.

[46] J.M. Feliu, A. Aldaz, P.A. Briand, F.- Meudon, Nature of Br Adlayers on Pt (111) Single-Crystal Surfaces . Voltammetric , Charge Displacement , and ex Situ STM Experiments, (1996) 2334–2344.

[47] N. Garc, E. Herrero, J.M. Feliu, On the electrochemical behavior of the Pt (1 0 0) vicinal surfaces in bromide solutions, 560 (2004) 269–284. doi:10.1016/j.susc.2004.04.051.

[48] S. Yoo, Y.A. Lei, X.C. Zeng, Effect of polarizability of halide anions on the ionic solvation in water clusters, J. Chem. Phys. 119 (2003) 6083–6091. doi:10.1063/1.1601609.

[49] B.E. Conway, B. Barnett, H. Angerstein-Kozlowska, B. V. Tilak, A surface-electrochemical basis for the direct logarithmic growth law for initial stages of extension of anodic oxide films formed at noble metals, J. Chem. Phys. 93 (1990) 8361–8373. doi:10.1063/1.459319.

[50] M. Wakisaka, H. Suzuki, S. Mitsui, H. Uchida, M. Watanabe, Identification and Quantification of Oxygen Species Adsorbed on Pt(111) Single-Crystal and Polycrystalline Pt Electrodes by Photoelectron Spectroscopy, Langmuir. 25 (2009) 1897–1900. doi:10.1021/la803050r.

[51] A. Berná, V. Climent, J.M. Feliu, New understanding of the nature of OH adsorption on Pt(1 1 1) electrodes, Electrochem. Commun. 9 (2007) 2789–2794. doi:10.1016/j.elecom.2007.09.018.

[52] A. Grimaud, W.T. Hong, J. Tarascon, Anionic redox processes for electrochemical devices, Nat. Publ. Gr. 15 (2016) 121–126. doi:10.1038/nmat4551.

[53] S.S. Laletina, M. Mamatkulov, E.A. Shor, V. V. Kaichev, A. Genest, I. V. Yudanov, N. Rösch, Size-Dependence of the Adsorption Energy of CO on Pt Nanoparticles: Tracing Two Intersecting Trends by DFT Calculations, J. Phys. Chem. C. 121 (2017) 17371–17377.

doi:10.1021/acs.jpcc.7b05580.